Piecewise potential application of Schroedinger's equation to HREM imaging

P. Fraundorf
Physics & Astronomy, U. Missouri-StL (63121), St. Louis, MO, USA

(Dated: September 2, 2002)

This exercise prompts calculation of the exit surface deBroglie phase shift created in a high energy electron plane wave, as it interacts with the projected potential along the beam direction in a thin specimen. Although electron intensity is not affected by the specimen as the beam traverses it in the "thin-specimen" or phase-object approximation, an elegant trick of electron optics takes advantage of interference between phase-modified exiting wavefronts downstream in the wavepath. As a result, with sufficiently good beam stability and aberration correction, this can result in an electron intensity map of relative exit surface deBroglie phase (hence of projected potential in the specimen) with sub-atomic lateral resolution (see most recently Batson et al.[1]).

I. INTRODUCTION

Consider a one-dimensional specimen potential of the form $V = -e\phi$ for z between 0 and specimen thickness T (call this Region II), with $V = 0$ elsewhere. Here ϕ is the average electric potential (work function) for the atoms in a beam-path column through a specimen film of thickness T, within which high energy electrons of kinetic energy $E_k = eV_r$ will be traveling in the z-direction. Typical experimental values might be work function $\phi = 10$ [volts], specimen thickness $T = 1$ [nanometers], and accelerating voltage $V_r = 300,000$ [electron volts]. This accelerating voltage results in near-relativistic electrons, although for the exercise we are neglect relativistic corrections. More generally, ϕ may be a function of z, and greater at locations near the core of atoms than between them, as shown in Fig 1. Given such a piecewise continuous potential, consider incident electron plane waves of the form $\Psi[z,t] = \psi[z]e^{-i\omega t} = Ae^{i(kz-\omega t)}$ traveling in the positive z-direction.

In the questions of the next five sections, select the correct answer or answers. The section following that provides examples of application for the result.

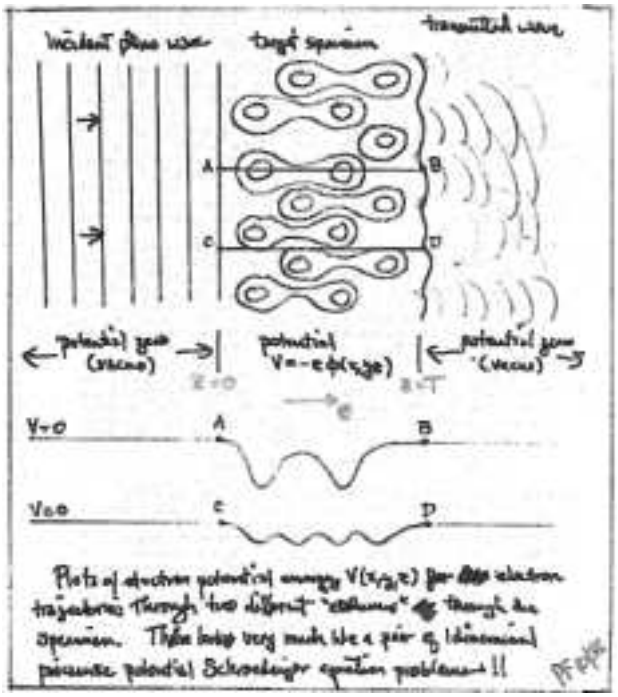

FIG. 1: In this exercise, we try to show that HREM images can be seen as maps of projected potential with sub-2[Angstrom] lateral resolution.

II. INCIDENT REGION

Solutions to the time-independent Schroedinger equation upstream of the specimen in the incident wavefield (i.e. when $z < 0$) might take which of the following forms?

- (A) $\psi[z] = Ae^{kz} + Be^{-kz}$,
- (B) $\psi[z] = Ae^{ikz} + Be^{-ikz}$,
- (C) $\psi[z] = Az^2 + Bz^{-2}$,
- (D) $\psi[z] = Ae^{ikz} + Be^{-kz}$.

III. THE SPECIMEN INTERIOR

The time-independent Schroedinger equation for Region II ($0 < z < T$) might be written $\psi[z] = Ce^{iKz} + De^{-iKz}$, where in terms of electron mass m, the wave vector K equals:

- (A) $\sqrt{\frac{2meV_r}{\hbar^2}}$,
- (B) $\sqrt{\frac{2me\phi}{\hbar^2}}$,

- (C) $\sqrt{\frac{2me(\phi+V_r)}{\hbar^2}}$,
- (D) $\sqrt{\frac{2me(V_r-\phi)}{\hbar^2}}$.

IV. SPECIMEN TOP SURFACE

Mathematical boundary conditions which apply at $z = 0$ include the following:

- (A) $A + B = C + D$,
- (B) $A - B = C - D$,
- (C) $ik(A + B) = iK(C + D)$,
- (D) $ik(A - B) = iK(C - D)$.

V. SPECIMEN EXIT SURFACE

Neglect relativistic contributions from ϕ, recognize that $\phi << V_r$ for high energy electrons, and define projected potential as $\Phi \equiv \int_0^T \phi dz$. Then the resulting exit surface ($z = T$) deBroglie phase shift σ, relative to that for a vacuum electron, can be written as...

- (A) $\int_0^T (K - k)dz$,
- (B) $k\int_0^T \left(\sqrt{1 + \frac{\phi}{V_r}} - 1\right) dz$,
- (C) $k\int_0^T \frac{\phi}{2V_r}dz$,
- (D) $\frac{k}{2V_r}\int_0^T \phi dz$,
- (E) $\frac{k}{2V_r}\Phi$.

VI. GETTING AN EXPERIMENTAL PREDICTION

Using the numbers given in the introduction, the deBroglie phase shift σ for a specimen which is only $T = 1$ [nm] (or about 5 atoms) thick would be approximately...

- (A) 0.01 radian,
- (B) 0.05 radian,
- (C) 0.1 radian,
- (D) 0.5 radian.

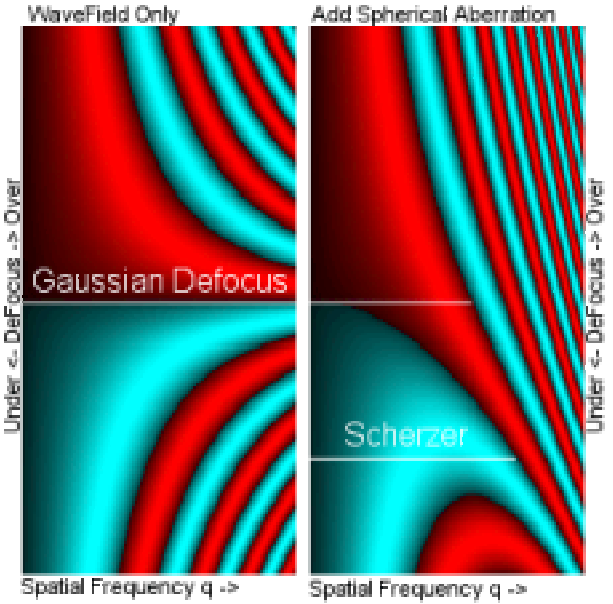

FIG. 2: Complex color plots of $sin[W]$ (cyan corresponds to positive phase contrast i.e. dark atoms, red to the opposite) as a function of defocus Δz from the specimen exit surface (vertical axis) versus spatial frequency q (horizontal axis). The left plot considers only propagation of the wavefield beneath the specimen, the right plot further takes into account spherical aberration in the microscope. Gaussian defocus refers to focus on the exit surface itself, Scherzer defocus corresponds to a traditional optimum setting chosen for real microscopes.

VII. RELATIVISTIC CORRECTIONS

At relativistic speeds, electron momentum goes from $p \simeq \sqrt{2m_eE_k}$ to $p = \sqrt{2E_k(E_o + E_k)}/c$. Here rest energy $E_o \equiv m_ec^2$, where c and m_e are lightspeed and electron rest-mass, respectively. Hence wavenumber $k = \frac{2\pi}{\lambda}$ is changed via the dependence of wavelength on momentum $\lambda = h/p$. Also, the ratio between wavelength outside the specimen to wavelength inside the specimen (i.e. the specimen's refractive index) changes subtly as well. Therefore the factor of $\frac{1}{2V_r}$, which multiplies projected potential to get the optical path difference, becomes $\frac{1}{V_r}\frac{E_o+E_k}{2E_o+E_k}$. Otherwise, the above analysis of phase shift remains intact[3,4].

VIII. WHAT HAPPENS NEXT?

Scattering in quantum mechanics results in an electron wave which is both phase shifted, and changed in direction. A classic use of the Born approximation, the WKB method, and partial wave analyses has been calculating the angular dependence of scattering from single atoms, based on the details of charge distribution within – Rutherford's famous discovery of the nucleus was an early consequence thereof. Fortunately for the electrons discussed here, these angular issues are less important

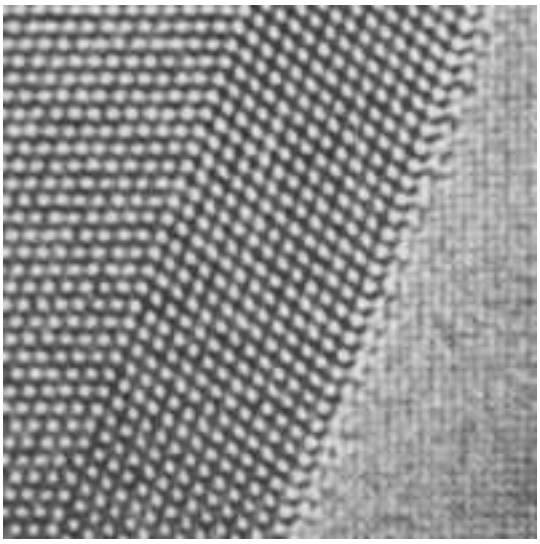

FIG. 3: An electron phase contrast image of the interface between an internally twinned fcc germanium precipitate, and the aluminum metal matrix in which it was formed, taken by the ARM at the National Center in Berkeley[2].

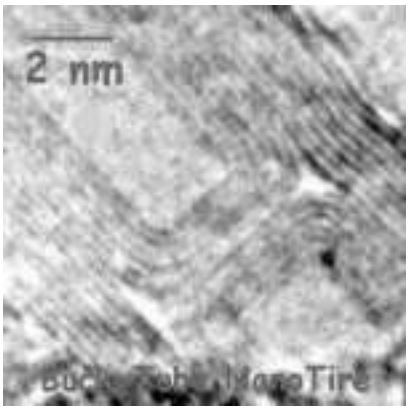

FIG. 4: An electron phase contrast image of the internal structure of a 15 wall carbon nanotube, the innermost 6 atomic layers of which form an internal closure. Taken with the EM430ST at UM-StL.

because scattering angles are well under 10 milliradians.

If one uses apertures which are large enough to include both scattered and unscattered beams (e.g. in the back focal plane of the objective lens, where exit surface waves are separated according to direction rather than amplitude), then one can imagine imaging the amplitude-added unscattered and scattered wavefields together (at least over specimen distances less than the transverse coherence width of incident electrons). Hence the first practical requirements for electron phase contrast imaging are thin specimens, moderate coherence width illumination, and large objective apertures.

Under these conditions, the imaged exit surface wave from a thin crystal looks like the incident wave, multiplied by $e^{+i\sigma}$, where $\sigma[x,y] \simeq \frac{k}{2V_r}\Phi[x,y]$ varies with lateral coordinate values x and y across the specimen. If the phase angle is small (i.e. much less than π), the multiplying factor can be approximated by $e^{+i\sigma} \simeq 1+i\sigma$.

Imagine a one dimensional specimen with only spatial frequency $q = 1/\Lambda$, where Λ is the repeat distance, e.g. so that $\sigma[x] = \sigma_o cos[2\pi qx]$. At the exit surface, the wavefield will have been multiplied by $\psi[x] = 1+i\sigma_o cos[2\pi qx]$. Note that, as long as $\sigma_o << 1$, the amplitude of the composite wave field is hardly affected by the specimen's periodicity. In light microscopy, this problem is overcome by inserting a Zernike phase plate[3] for shifting the scattered beam only by an additional $\pi/2$, resulting (when recombined) in first order amplitude effects.

In the absence of a suitable phase plate, one can instead defocus one's imaging optics so as to sample the wavefield downstream (or virtually, upstream as well) from the exit surface of the specimen, at a point where phase differences at the exit surface interfere with one another to create ripples in intensity which may be photographed. What defocus setting is appropriate depends on the spatial frequencies of interest.

Physically, the scattered wavefield evolves by convolution with the Fresnel propagator, which is oft written (apart from a constant factor[4,5]) as $e^{\frac{i\pi(x^2+y^2)}{\lambda\Delta z}}$. Here Δz is the distance from the exit-surface along the beam direction, or the "defocus setting", defined so as to be positive in the downstream (underfocus) direction. In frequency space, this is equivalent to multiplying the wavefield by the propagator's Fourier transform, the transfer function e^{-iW} defined here in terms of the "defocus function" $W[\Delta z] = \pi\lambda\Delta z(q_x^2 + q_y^2)$. For our single frequency specimen, the imaged amplitude is thus modulated by $\psi = 1 + ie^{-iW}\sigma_o cos[2\pi qx]$. The intensity found in the image becomes $I \equiv \psi^*\psi = 1 + 2sin[W]\sigma_o cos[2\pi qx]$.

The factor $sin[W]$, a function of both defocus Δz and spatial frequency q, thus determines both the strength and sign of intensity ripples corresponding to specimen structure, in the captured image. It predicts dark spots in the neighborhood of large phase shifts (e.g. atom columns), for example when W is near $-\pi/2$. We also might want to choose defocus Δz so that the images are simplest to interpret, e.g. so that $sin[W]$ is finite and constant for as wide a range of frequencies as possible. To assist with this, we've plotted $sin[W]$ as a function of transverse spatial frequency q, and defocus Δz, for unit wavelength on the left hand side of Figure 2.

Spherical aberration in the objective lens also affects the image. The effect is shown graphically on the right hand side of Figure 2. Since zeros in $sin[W]$ correspond to phase reversals for the corresponding periodicity, a traditional goal has been to select a defocus for which these zero's are moved outward to as high a frequency as possible. As illustrated in the diagram, Scherzer defocus is the setting of choice in this regard. Recent work has concentrated on combining images taken at multiple defocus settings into even higher resolution composites. For example, the "One Angstrom Microscope"

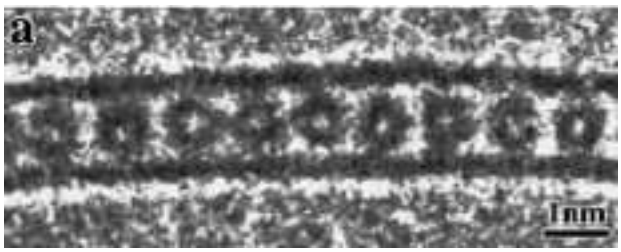

FIG. 5: Single walled carbon nanotube filled with buckyballs, from Hirahara et al.[6].

at Lawrence Berkeley Labs can apparently take images with 0.8 Angstrom resolution, even though the first zero in it's optics corresponds to a resolution of nearer to 1.7 Angstroms.

For quantitative microscopy of thicker specimens in real microscopes, of course, other issues must be considered as well: e.g. vibration and electrical instabilities, knowledge of specimen thickness, astigmatism, and the range of illumination angles in the beam. Even then the theory remains quite elegant, and except for the effects of specimen thickness can be visualized by changes in the fingerprint of Fig 2.

Of course, this analysis might seem abstract. Au contraire! Recall that amorphous materials in projection are, unlike crystals, likely to show a uniform distribution of periodicities. As a result, the zeros of the imaginary part of the Fresnel transfer function, for the current defocus setting in the right side of Fig 2, show up as rings in the power spectrum from amorphous material *in every HREM image*.

IX. ELECTRON PHASE CONTRAST IN ACTION

Figure 3 is a mechanically thinned metallurgical specimen. If the thin specimen approximation were valid here, white dots would correspond to tunnels between atom columns. Fig 4 is closeup of a multiwall carbon nanotube, whose internal closure results in formation of a toroidal void circling the tube axis: Perhaps one of the world's smallest manmade "inner tubes". Fig 5 shows bucky balls lined up inside a single-walled carbon nanotube. The atom-thick surfaces are darker when edge-on because of their greater projected potential.

REFERENCES

[1] P. E. Batson, N. Delby, and O. L. Krivanek, Nature **418**, 617 (2002).

[2] U. Dahmen, Bull. Electron Microscope Soc. Amer. cover **16**(2), 5 (1986).

[3] L. Reimer, *Transmission electron microscopy: Physics of image formation and microanalysis* (Springer-Verlag, Berlin, 1997), 4th ed.

[4] J. C. H. Spence, *Experimental High-Resolution Electron Microscopy* (Oxford University Press, New York, 1988), 2nd ed.

[5] J. D. Gaskill, *Linear systems, Fourier transforms, and optics* (John Wiley and Sons, New York, 1978).

[6] K. Hirahara, S. Bandow, K. Suenaga, H. Kato, T. Okazaki, H. Shinohara, and S. Iijima, Phys. Rev. B **64**, 115420 (2001).